The Transfer of Strike-Slip Partitioned Motion of Oblique Convergence Across the Zagros Fold-and-Thrust Belt

C. Authemayou[1], O. Bellier[1], D. Chardon[1], Z. Malekzade[2], M. Abassi[2], and E. Shabanian[2]

1. Centre Européen de Recherche et d'Enseignement de Géosciences de l'Environnement (UMR CNRS 6635), Université Aix-Marseille 3, BP 80, 13545 Aix-en-Provence Cedex 4, France
   email: authemayou@cerege.fr
2. International Institute of Earthquake Engineering and Seismology (IIEES), Tehran, I.R. Iran

ABSTRACT: *Oblique plate convergence in collision zones may lead to complex regional strain partitioning because inherited crustal faults have various orientations with respect to the orogenic belt and the convergence vector. Combined field structural and geomorphic investigations and SPOT image analysis document the kinematic framework enhancing transfer of strike-slip partitioned right-lateral motion from along the backstop to the interior of the Zagros fold-and-thrust belt in a context of active, high-angle right-oblique plate convergence. Transfer occurs by slip on the N-trending right-lateral Kazerun fault system that connects to the termination of the Main Recent Fault, a major NW-trending dextral fault partitioning oblique convergence at the rear of the belt. The Kazerun Fault system consists in three N-trending fault zones ended by bent, orogen-parallel splay thrust faults allowing slip from along the Main Recent Fault to become distributed by transfer to longitudinal thrust faults and folds.*

Keywords: Zagros; Strike-slip fault; Kazerun fault system; Segmentation; Fault kinematics

1. Introduction

In oblique plate convergence, deformation may be partitioned between orogen-parallel strike-slip faults and thrusts [1]. This mechanism has been mainly documented along subduction zones e.g., [2, 3], and more rarely in collisional settings e.g., [4] although oblique convergence must be common in active and fossil collision zones. The Zagros fold-and-thrust belt of Southern Iran is a young active collisional orogen that provides a particularly relevant case-study for examining the relations between far-field boundary conditions and internal strain partitioning within a mountain belt.

In this paper, we present an integrated study of part of the Zagros fold-and-thrust belt combining field structural and geomorphic investigation and *SPOT* satellite image analysis. The aim of this work is to assess the recent active geometry and kinematics of the Kazerun Fault System (*KFS*), one of the longest *NNE*-trending active strike-slip faults in the Zagros that crosscuts the entire belt at a high angle [5-7]. This allows addressing its relations to active thrusting and orogen-parallel, strike-slip partitioned motion at the backstop of the fold-and-thrust belt in the frame of high-angle right-oblique convergence.

2. Geodynamic Setting

The *NW*-trending Zagros fold-and-thrust belt results from the Neogene collision between the Arabian and Eurasian plates e.g. [8-9]. The belt stretches from eastern Turkey to the Oman Gulf, see Figure (1). The northeastern boundary of the belt coincides with the Main Zagros Reverse Fault (*MZRF*) that

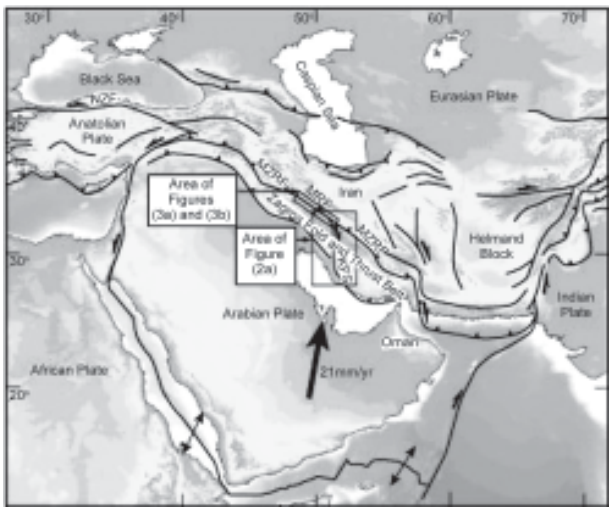

Figure 1. Structural frame of the Middle-East portion of the Alpine collision belt showing the plate convergence vector relative to Eurasia [13-14]. NAF-North Anatolian fault; MZRF-Main Zagros reverse fault; MRF-Main recent fault; and KFS-Kazerun fault system.

represents the backstop of the fold-and-thrust belt [8, 10], see Figure (1).

According to *GPS* measurements, the Arabian and Eurasian plates converge at 21*mm/yr* c.a. 50°*E* [11-13], see Figure (1). At this longitude, the Zagros records a *NNE*-trending shortening rate of about 10*mm/yr* that is oblique with respect to the main fold-and-thrust belt strike [14], see Figure (1). Earthquake focal mechanisms [5, 15, 16] indicate that a significant part of the convergence obliquity is turned into slip on the *NW*-trending Main Recent Fault (*MRF*), that runs south of, and parallel to the *MZRF* at least as far as 51°*E* to the east [17]. This fault accommodates the orogen-parallel, dextral strike-slip component of the oblique plate convergence at the rear of the Zagros fold-and-thrust belt at a rate of 10-17*mm/yr* (estimate by Talebian and Jackson, [18]).

A set of N-trending faults recognized as inherited basement structures, disrupts the *NW*-trending longitudinal Zagros folds [19-22]. Geomorphic evidence and focal mechanisms indicate that these right-lateral strike-slip faults are active and affect both the cover and basement of the belt [6, 7, 23], see Figure (2a). The most prominent of these faults is the *KFS* that stretches from the eastern termination of the *MRF*, in the north, to the Persian Gulf, in the south. The fault marks the boundary between two drastically different structural domains. The width of the belt west of the *KFS* is narrow (200*km*), salt extrusions are lacking suggesting the absence of the Hormuz Salt at depth [21] and earthquakes are localised on major thrust faults e.g., [5]. By contrast, to the east of the fault, earthquakes are distributed throughout the 300*km*-width of the Zagros fold-and-thrust belt [5, 16, 24]. According to seismicity data, the *KFS* is active with a high level of seismicity along its central part, where historical earthquakes of intensity reaching *VIII* have been reported [6, 25, 26], see Figure (2a).

3. Kazerun Fault Segmentation

Our work, combining *SPOT* images analysis, compilation of existing geological maps and new field observations and data, allows a reassessment of the fault trace proposed by previous workers [5, 7, 21, 28, 27] by producing the first detailed map of its active segmentation.

The *KFS* is made of three north-trending fault zones of equivalent length (~100*km*-long). They have similar trace shapes with a general *N*170-180°*E*-trend and a southern termination bent towards *SE* strikes, see Figure (2b). Their terminations spilt as bend splays and are generally connected eastward to the *NW*-trending thrust and ramp anticlines whose forelimbs are systematically overturned close to the *KFS*, implying an increase in south verging reverse-slip along the ramps towards the *KFS*.

The northern fault zone comprises five ~40*km*-long segments. The northernmost one reaches the eastern tip of the *MRF* through a narrow discontinuity arranged in a relay fault bend, see Figure (2b). 30*km* further south, the High Zagros Fault (*HZF*) [25] merges with the northern segment close to the only releasing stepover of the fault zone, see Figure (2b). The central fault zone comprises seven segments with an average trend of *N*02°*E*, a majority of discontinuities between the segments being restraining stepovers, see Figure (2b). Contrary to the northern fault zones, several segments of the southern fault zone are arranged in an en echelon pattern and the northernmost one is bent towards *NW* strikes into a thrust, see Figure (2b). This thrust fault makes up the Zagros front west of the *KFS* [5] that is shifted 100*km* southward, east of the *KFS*. Bending of a large coastal anticline seen *SW* of Khormuj suggests the presence of a hidden, *N*-trending prolongation of the southern segment of the *KFS* at least up to the coast, see Figure (2b). It is interesting to note that, although fault zone lengths are comparable, large-scale segmentation displays a

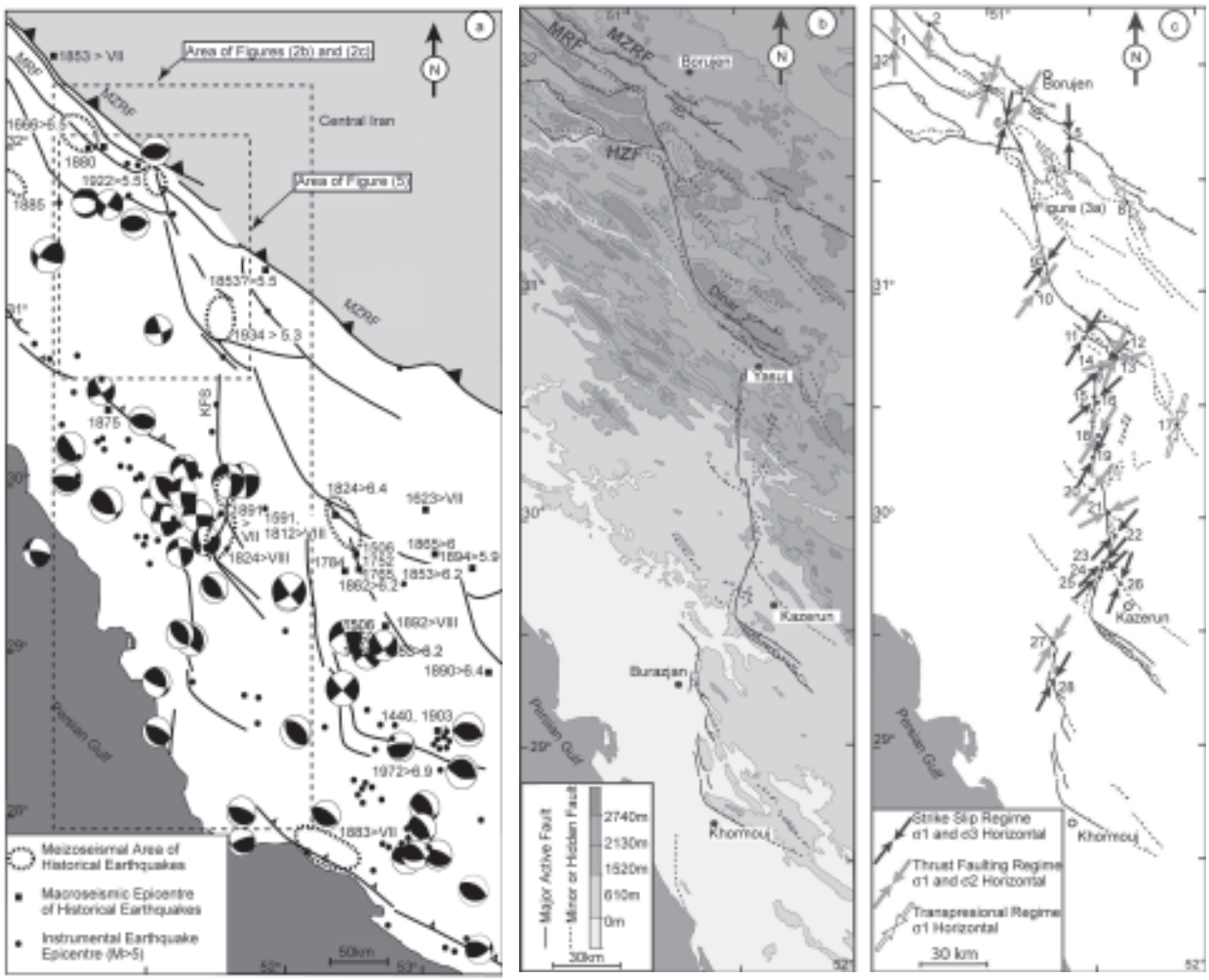

Figure 2. (a) Compilation of shallow earthquakes (< 60-km-depth) epicenters and focal mechanisms in the Zagros fold-and-thrust belt between 50 and 54°E [5, 25, 51] superimposed on a fault pattern deduced from LANDSAT image interpretation (located on Figure (1)). Fault-plane solutions were calculated following the Centroid Moment Tensor method (CMT) from the Harvard list. (b) Active segmentation of the Kazerun Fault system superimposed on topography. (c) Result of the fault-slip data inversion along the Kazerun Fault system. Arrows represent the σ1 axis strike and station numbers refer to Table (1). Frame of Figures (2b) and (2c) are located on Figure (2a).

northward increase in the segment length implying an increasing segmentation complexity southward.

4. Southeastern Main Recent Fault Segmentation

In order to evaluate the respective role between the *NW*-trending *MRF* and the *N*-trending *KFS*, a detailed mapping of the surface fault trace on the southeastern *MRF* region was conducted. The southeastern *MRF* is characterized by a single segment in the Dorud region cutting across thrust sheets shown in Figure (3a). These thrust sheets consist on metamorphic rocks coming from Central Iran. They ceased to be active during the early Pliocene [48]. These relationships indicate that *MRF* strike-slip movement has been initiated during early Pliocene. Southeastward, the *MRF* splits into two 180*km*-long major fault zones 15*km* apart, as shown in Figure (3a). Near the *KFS*, the southern *MRF* fault zone is bent northeastward, joining the northern *MRF* zones that connect with the *KFS* northern tip, as shown in Figure (3b). The longest segment is located on the southern fault zone measuring 130*km*-long. Preliminary analysis of Quaternary geomorphic feature offsets (streams and associated alluvial fans) along the two *MRF* fault zones suggest a significant horizontal slip along the southern *MRF* fault zone. In Figure (3) two sites located on each fault zone, where stream offsets are clearly representative of the geomorphic feature offset all along the fault zone, are illustrated. On the site of the northern fault zone, as shown in Figure (3b), stream offsets affecting alluvial fans are of the order of 75*m*, see Figure (4a). On the site of the southern

Table 1. Location of fault measurement sites, results of stress-tensor inversions from slip-data, and age of the faulted formations at each site. Inversion results include the orientation (azimuth and plunge) of the principal stress axes and R, a stress ellipsoid shape parameter. Principal stress axes, σ1, σ2 and σ3, correspond to the compressional, intermediate and extensional deviatoric stress axes, respectively, and R is defined as R = (σ2 - σ1)/(σ3- σ1)).

Site	Latitude	Longitude	N	σ1 Az-Pl	σ2 Az-Pl	σ3 Az-Pl	R	Age
1	32°01'871	50°37'819	22	182-7	356-83	92-1	0,4	Quaternary Conglomerate
2	32°11' 223	50°43' 308	11	359-17	266-10	146-70	0,921	Cretaceous Marl-Limestone
3	31°54' 941	51°00' 007	15	198-5	288-1	24-85	0,229	Plio-Quaternary Conglomerate
4	31°51' 648	51°09' 873	6	209-0	119-0	311-90	0,276	Cretaceous Marl-Limestone + Plio-Quaternary Conglomerate
5	31°41' 996	51°23' 443	5	179-0	81-90	269-0	0,871	Cretaceous Marl-Limestone
6	31°45' 523	51°05' 747	12	193-0	51-90	283-0	0,323	Cretaceous Marl-Limestone
7	31°31'746	51°21'913	24	148-9	49-45	247-43	0,991	Miocene Conglomerate Sandstone, Marl
8	31°24'108	51°39'320	21	148-0	58-57	239-33	0,625	Miocene Conglomerate Sandstone, Marl
9	31°07' 457	51°16' 288	22	216-11	100-66	311-21	0,48	Jurassic Dolomite
10	31°06' 913	51°12' 137	11	215-18	118-23	339-60	0,782	Miocene Red Marl
11	30°53' 676	51°23' 014	17	210-8	83-76	302-11	0,365	Plio-Quaternary Conglomerate
12	30°42'571	51°36'119	16	201-11	292-7	52-77	0,941	Plio-Quaternary Conglomerate
13	31°42' 082	51°33' 123	6	74-0	164-0	343-90	0,943	Plio-Quaternary Conglomerate
14	30°40' 621	51°31' 594	6	46-0	136-89	316-1	0,956	Oligo-Miocene Dolomite + Quaternary Conglomerate
15.16	30°27' 425 30°33' 002	51°30 931 51°30' 578	20	227-12	330-47	126-41	0,148	Oligo-Miocene Dolomite
17	30°30'103	51°51'236	18	17-39	220-49	116-12	0,192	Upper Cretaceous Dolomite
18	30°22' 818	51°28' 998	11	31-10	300-4	189-80	0,959	Upper Cretaceous Limestone
19	30°18' 719	51°30' 147	13	27-10	290-36	130-53	0,741	Upper Cretaceous Limestone
20	30°07' 622	51°29' 576	4	219-0	129-0	311-90	0,705	Plio-Quaternary Conglomerate
21	30°02' 378	51°32' 879	12	242-3	332-2	97-87	0,972	Upper Cretaceous Limestone
22	29°55' 927	51°35' 440	6	40-18	250-70	133-10	0,466	Upper Cretaceous Limestone
23	29°49' 261	51°32' 738	14	221-0	131-89	311-1	0,98	Oligo-Miocene Dolomite + Quaternary Conglomerate
24	29°46' 882	51°31' 551	12	224-6	105-78	315-10	0,107	Oligo-Miocene Dolomite
25	29°45' 862	51°31' 477	16	224-18	98-61	321-22	0,801	Oligo-Miocene Dolomite
26	29°41' 007	51°38' 723	10	30-10	246-78	121-7	0,833	Quaternary Conglomerate
27	29°28' 227	51°16' 587	6	28-7	119-8	255-79	0,253	Plio-Quaternary Conglomerate
28	29°16' 403	51°16' 747	8	205-7	53-82	295-4	0,513	Oligo-Miocene Dolomite + Quaternary Conglomerate

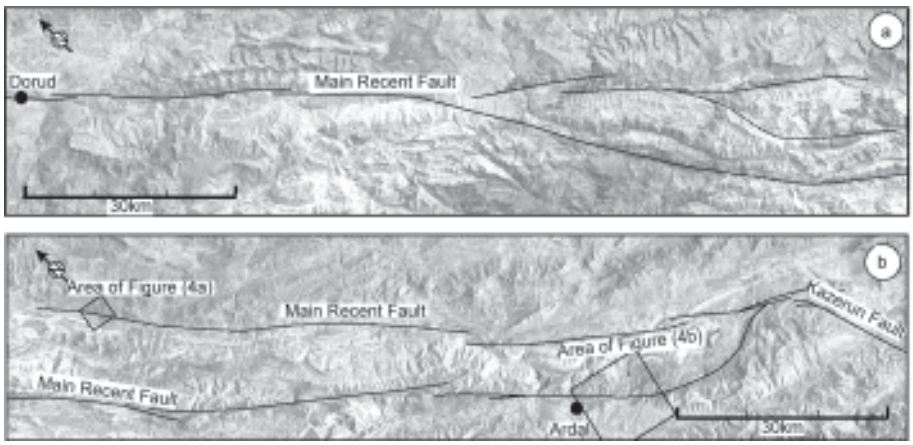

Figure 3. (a) Active segmentation of the western part of southeastern termination of the MRF. (b) Active segmentation of the eastern part of southeastern termination of the MRF. Frame of Figures (3a) and (3b) are located on Figure (1).

fault zone, two orders of right-lateral stream offsets were identified: 650*m* and 1300*m*, as shown in Figure (4b). The longer stream offset (1300*m*-long) is associated with the largest drainage basin surface suggesting an onset of this offset older than the one of the stream offset of 650*m*.

5. Fault Kinematics and Stress Regime

The *N*-trending northern and central fault zones of the *KFS* exhibit evidence for active right-lateral slip (offset of Quaternary streams and alluvial fans, occurrence of pressure ridges; shown in Figure (5a)) whereas in the *NW*-trending splay fault zone terminations, uplifted and tilted benches or Quaternary alluvial terraces are documented, see Figure (5b). This indicates a dominant active strike-slip component on the *N*-trending segments and a reverse dip- to oblique-slip component on the fault zone terminations.

In order to further constrain the tectonic regime of the fault and the associated stress states, a fault kinematic study at 28 sites distributed along the fault system was performed. An inversion of each fault slip data has been performed using the method originally proposed by Carey [29], see Figure (6a). Fault slip-vector inversions, presented in Figure (2c), indicate a consistent right-lateral strike-slip regime all along the *KFS* with a thrust-faulting regime around the bent splay fault zone terminations. Regionally significant stress states were calculated using two methods. The first one results from a statistical analysis of the stress states previously obtained at each site. The second one was computed by inversion of major fault planes slip measurements. Both methods led to consistent results that are also in agreement with a strike-slip stress regime characterised by a $N35\text{-}40°E$-trending $\sigma 1$, see Figure (6b). On the two southern fault zones, the strike-slip striations compatible with this stress

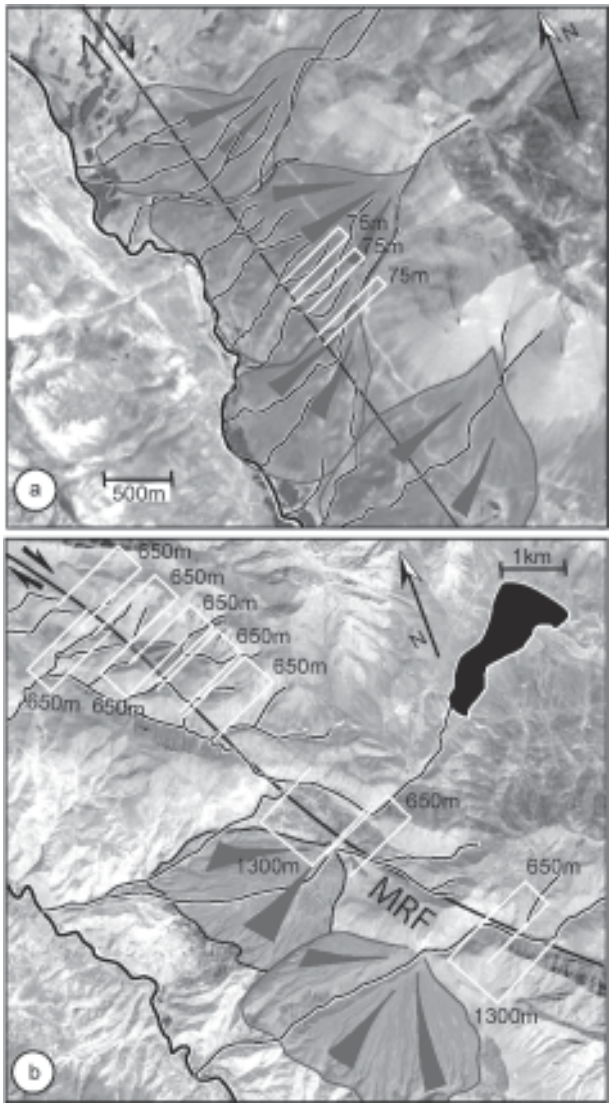

Figure 4. (a) SPOT satellite image of the northeastern fault zone of the MRF with the drainage offsets of the order of 75 m and the alluvial fans. (b) SPOT satellite image of the southeastern fault zone of the MRF with the two orders of stream offsets and the alluvial fans. Frame of Figures (4a) and (4b) are located on Figure (3b).

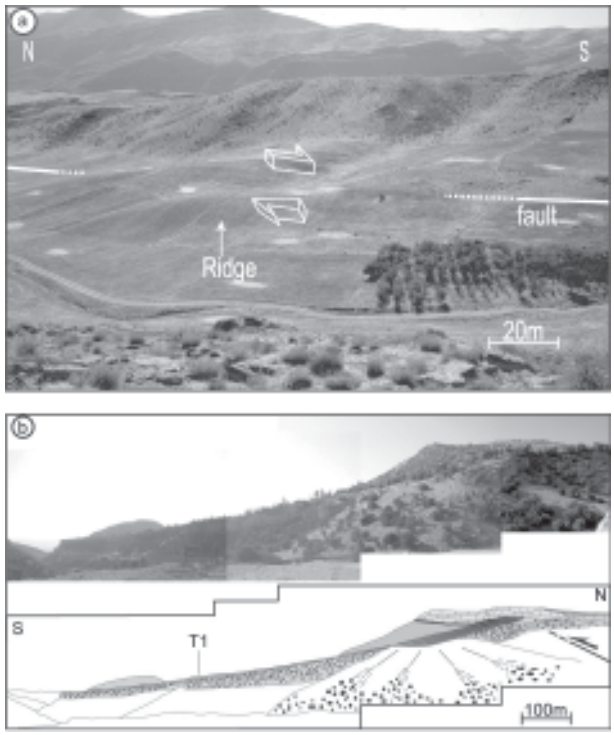

Figure 5. (a) View of the KFS scarp showing stream offset and dextral pressure ridge on the northern fault zone (located on Figure (2c)). (b) View of the Dinar thrust fault (northern KFS fault zone) showing tilted and folded late Quaternary Terrace (station 11, Figure (2c)).

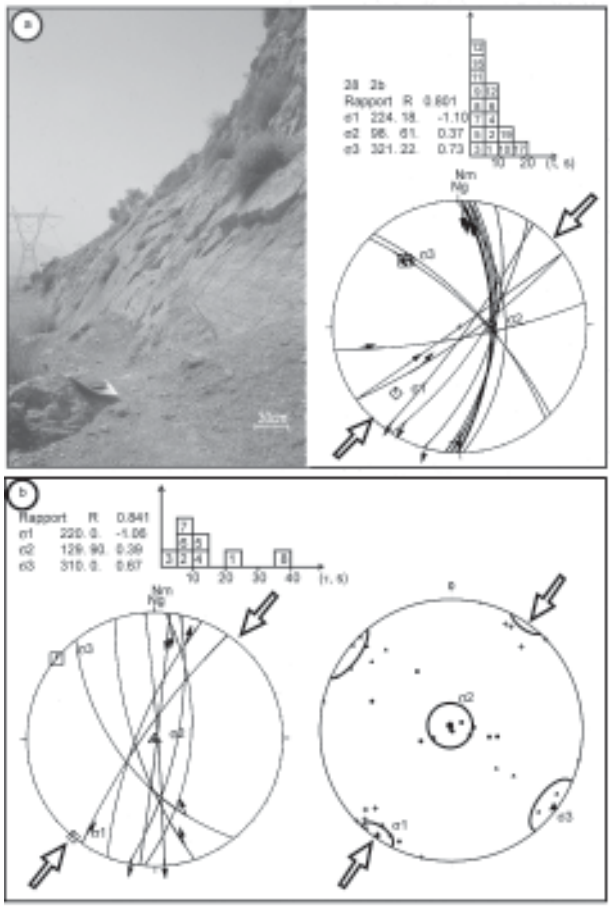

Figure 6. (a) Example of a type locality along the central fault zone. View, looking south, of station 25 and corresponding fault-slip data (lower hemisphere stereonet) and inversion results (see Table (1) for explanation). (b) Major fault planes striations measured along the KFS and their inversion result (left) and regional significant stress state (right) obtained from a statistical method computing the mean stress axes (with their 95% confidence cones) using the McFadden's method computed with PMSTAT software [52].

Figure 7. (a) Structural map of the Borujen region based on SPOT image interpretation, our field observations and published geological maps (see references in the text). (b) Shortening (normal to the fold axis) trajectories superimposed on the main structures. Note that the two fault kinematic measurement sites showing deviation from the homogeneous stress state shown in Figure (2c) are located along the MZRF and at the northern most KFS site, see Figures (2c) and (5b). They are interpreted to result from the interference pattern shown here by the trajectories.

regime were measured on fault planes affecting Jurassic to Plio-Quaternary formations as well as recent alluvial and colluvial deposits. There appears to be no significant temporal changes in the stress state along the two southern fault zones despite the long and complex history of the fault system [30]. While these inversion results are also consistent with earthquake focal mechanisms, as shown in Figure (2a), they are interpreted to reflect the present-day stress regime.

6. Structural Relations at the Rear of the Fold-and-Thrust Belt

In order to address the relations between the *KFS*, the *MRF*, and the *MZRF*, a detailed structural map covering their interaction zone, see Figure (7), based on *SPOT* images analysis, field observations and available geological maps was compiled [31-37]. The rectilinear *MZRF* marks the northern limit of the interference zone. At its southeastern tip, the *MRF* gives way to the *NNW*-trending northernmost segment of the *KFS* and to the dextral, oblique-reverse Semirom fault that trends at a low angle with respect to the eastern termination of the *MRF*, see Figure (7). The *GPS* measurements and seismologic data provide evidence for no significant activity along the *MZRF* [13, 26, 38]. This appears to be confirmed by our own geomorphological observations in the Borujen area. Consequently, this structural arrangement, as shown in Figure (7), implies that the cumulated slip of the two strands of the *MRF* is transmitted to both the *KFS* and Semirom faults. These faults, together with the main segment of the northern *KFS* fault zone, define a wedge-shape domain, see Figure (7). In the inner part of that wedge, the southwestern termination of the northernmost segment of the *KFS* merges into a *SE*-verging thrust. Within the wedge, finite

shortening trajectories are perturbed, suggesting an interference pattern around the bounding strike-slip and internal thrust fault. This results from superimposed deformation patterns involving potential anticlockwise rotations, dextral-oblique reverse (i.e., transpressional) slip along the Semirom fault, dextral slip along the *KFS*, as well as differential displacements between these two faults.

7. Discussion-Conclusion

The finite pattern described above has been produced in two stages, see Figure (8): an early phase of westward reverse dip-slip along the northern Kazerun fault zone and a younger phase of strike-slip documented in the present study in relation with the *MRF/KFS* connection. Evidence for the first phase regime is based 1) on the occurrence of exhumed Jurassic formations on the hanging wall whilst they are deeply buried (at c.a. minimum 5*km*-depth, [39]) west of the fault [36]; 2) the 5- to 9*km*-offset of the top of the basement across the fault [40]. These movements started as early as the Late Cretaceous, at the time the northern *KFS* was the tectonic front of the High Zagros belt [9, 26, 41, 42].

The second deformation phase that initiated strike-slip along the northern *KFS* is related to the onset of slip along the *MRF*. Anticlockwise rotation of Arabia allowed the *MRF* to propagate southeastward from the main Arabian indenter to reach and activate dextral strike-slip along the inherited *KFS*. This event is classically interpreted to have taken place around 5*Ma* ago [18], as a result of a regional re-organisation of the Arabia-Eurasia collision [43-47]. Indeed, field relationships from the central part of the *MRF* indicate that strike-slip initiated during the early Pliocene (i.e., during the deposition of the lower Bakhtiari formation) [48].

At that same time, the Semirom fault was activated and started transmitting part of the slip from the *MRF*, while the northern *KFS* absorbed the remaining part of horizontal strike-slip from along the *MRF*. Subsequent southeastward motion of the eastern *KFS* compartment south of the stationary *MZRF* produced southeastward thrusting within the wedge and *NW*-trending shortening across the Semirom fault as attested to by the fault kinematic analysis, see Figure (2c). Orogen-parallel dextral slip from along the *MRF* is therefore transmitted to the fold-and-thrust belt along *NW*-trending dextral transpressional faults and related folds (slightly oblique to the Main Zagros trend) and along the *N*-trending dextral, northern fault zone of the *KFS* and its southern thrust termination.

The structural and kinematic patterns shown in Figure (8) may be extrapolated to the scale of the Zagros fold-and-thrust belt, see Figure (9). Indeed, the structural wedge described in the Borujen area widens to the *SE* into a regional fan-shape fault pattern bounded to the west by the *KFS*, see Figure (8) [5, 28, 49]. We interpret this pattern to reflect distribution of slip from along the *MRF* to the

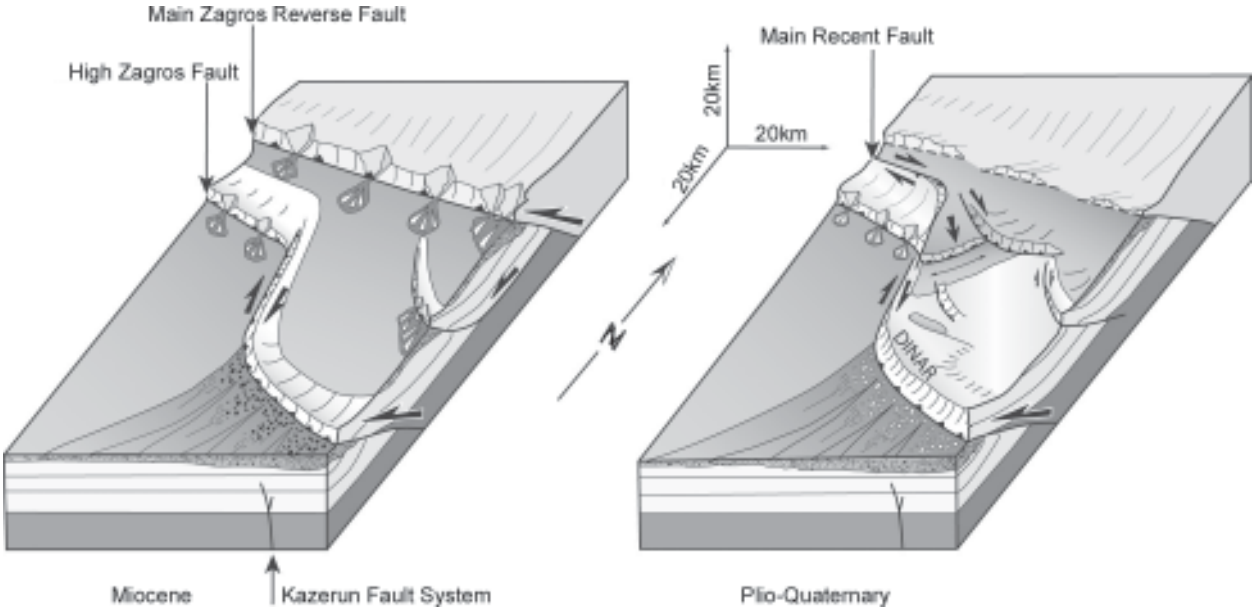

Figure 8. Block diagrams showing the two-stage evolution model of the northern KFS.

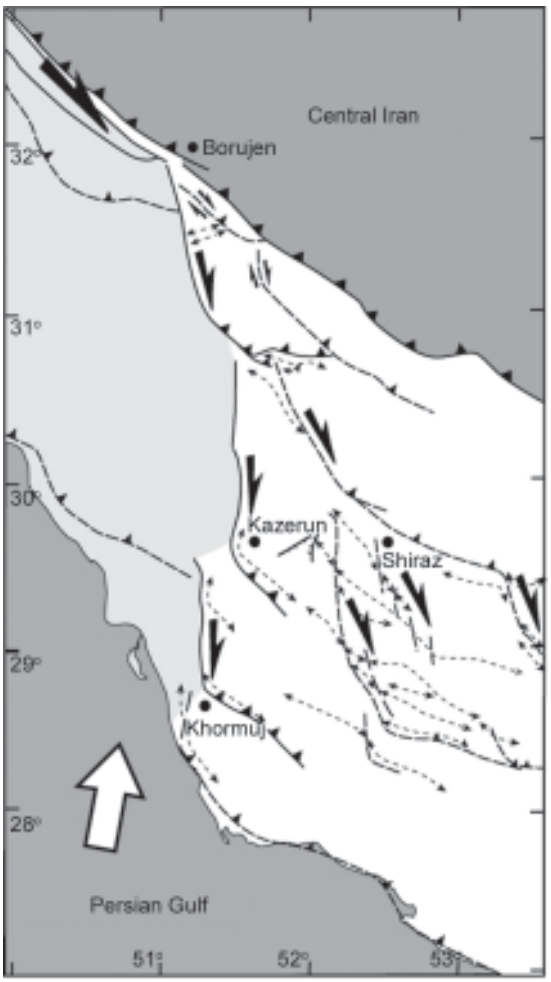

Figure 9. Synthetic map of the fault system distributing slip of the Main Recent fault to the Zagros fold-and-thrust belt. Deflected axial traces of anticlines are also shown.

fold-and-thrust belt through the thrust terminations of all these strike-slip faults of the fan. The Hormuz salt formation that assists slip distribution throughout the belt to the east of the *KFS* permits the southward migration of the Zagros front, and acts as a low-resistance boundary allowing the extrusion-like process produced by transfer of orogen-parallel slip to the belt.

The northward increase of the lateral Quaternary slip along the *KFS* suggested by preliminary first-order geomorphic observations may indicate southward decrease in the amount of slip transferred to the fold-and-thrust belt with low activity near the Persian Gulf coast. This is currently being tested by geochronological dating of offset alluvial fans.

The model presented here is kinematically compatible with previous interpretations of active slip along the *KFS*. Blanc et al [50] and Talebian and Jackson, [16] divide the Zagros fold-and-thrust belt into three zones which develop specific responses to plate convergence. Overall normal convergence is being recorded across the belt east of the fan-shape fault pattern whilst high-angle right oblique convergence would be active to the west of the *KFS*. The third zone would correspond to the fan shape fault pattern itself. Induced anticlockwise rotations and along-strike stretching of the belt east of the *KFS* [6, 16, 49] are achieved through this fan-shape fault pattern that displays distributed seismicity [16, 24].

The strike-slip partitioned motion of oblique plate convergence that is achieved by slip along the *MRF* within the western zone is transmitted and distributed to the central and eastern zones by slip along the *KFS* and associated faults. This fault system may therefore be seen as an orogen-scale, horse-tail like, strike-slip fault termination. In that sense, the *KFS* contributes to the fault system allowing partitioning of oblique convergence across the Middle-East Alpine collision belt and Arabia plate rotation associated with the westward extrusion of Anatolia [18] by transferring and distributing orogen-parallel dextral slip into the thrusts and folds of its frontal fold-and-thrust belt.

Acknowledgments

This work was funded by the Intérieur de la Terre and Dyeti programs (*INSU-CNRS*, France) and the International Institute of Earthquake Engineering and Seismology (*IIEES*, Tehran, Iran). We thank D. Hatzfeld and M. Ghafory-Ashtiany for supervising the program and M. Mokhtari for support and administrative assistance as well as K. Hessami for fruitful discussions, comments and logistical help. *SPOT* images (© *CNES*) were provided, thanks to the *ISIS* program.

References

1. Teyssier, C., Tikoff, B., and Markley, M. (1995). "Oblique Plate Motion and Continental Tectonics", *Geology.*, **23**, 447-450.

2. Fitch, T.J. (1972). "Plate Convergence, Transcurrent Faults, and Internal Deformation Adjacent to Southeast Asia and Western Pacific", *J. Geophys. Res.*, **77**, 4432-4460.

3. Bellier, O. and Sebrier, M. (1995). "Is the Slip Data on the Great Sumatran Fault Accommodated by Fore-Arc Stretching?", *Geoph. Res. Lett.*, **22**, 1969-1972.

4. Gaudemer, Y., Tapponnier, P., Meyer, B., Peltzer, G., Shunmin, C., Zhitai, D.H., and Cifuentes, I., (1995). "Partitioning of Crustal Slip between Linked, Active Faults in the Eastern Qilian Shan, and Evidence for a Major Seismic Gap, the 'Tianzhu Gap', on the Western Haiyuan Fault, Ganzu (China)", *Geophys. J. Int.*, **120**, 599-645.

5. Berberian, M. (1995). "Master Blind Thrust Faults Hidden under the Zagros Folds: Active Basement Tectonics and Surface Morpho-tectonics", *Tectonophysics*, **241**, 193-224.

6. Baker, C., Jackson, J., and Priestley, K. (1993). "Earthquakes on the Kazerun Line in the Zagros Mountains of Iran: Strike-Slip Faulting within a Fold-and Thrust Belt", *Geophys. J. Int.*, **115**, 41-61.

7. Bachmanov, D.M., Trifonov, V.G., Hessami, Kh.T., Kozhurin, Ivanova, T.P., Rogozhin, E.A., Hademi, M.C., and Jamali, F.H. (2004). "Active Faults in the Zagros and Central Iran", *Tectonophysics*, **380**, 221-241.

8. Stöcklin, J. (1968). "Structural History and Tectonics of Iran", A Review. Am. Ass. Petrol. Geol. Bull., **52**, 1229-1258.

9. Falcon, N. L. (1974). "Southern Iran: Zagros Mountains. In: Mesozoic-Cenozoic Orogenic Belts", (Spencer, A., ed.), Spec. Publ. Geol. Soc. London, **4**, 199-211.

10. Stöcklin, J. (1974). "Possible Ancient Continental Margins in Iran", Geology of Continental Margins (Burk, C. and Drake, C., eds.), Springer-Verlag, New York, 873-887.

11. McClusky, S.M., Balassanian, S., Barka, A., Demir, C., Ergintav, S., Georgiev, I., Gurkan, O., Hamburger, M., Hurst, K., Kahle, H., Kasten, K., Kekelidze, G., King, R.W., Kotzev, V., Lenk, O., Mahmoud, S., Mishin, A., Nadariya, M., Ouzimis, Paradissis, D., Peter, Y., Prilepin, M., Reillinger, R., Sanli, I., Seeger, H., Tealeb, A., Toksöv, M.N., and Veis, G. (2000). "Global Positioning System Constrains on Plate Kinematics and Dynamics in the Eastern Mediterranean and Caucasus", *J. Geophys. Res.*, **105**, 5695-5719.

12. Sella, G.F., Dixon, T.H., and Mao, A. (2002). REVEL: A Model for Recent Plate Velocities from Space Geodesy", *J. Geophys. Res.*, **107**(B4), ETG 11-1, 11-32.

13. Tatar, M., Haztfeld, D., Martinod, J., Walpersdorf, A., Ghafory-Ashtiany, M., and Chéry, J. (2002). "The Present-Day Deformation of the Central Zagros from GPS Measurements", *Geophys. Res. Lett.*, **29** (19), 1927, doi:10. 1029/2002GL015427.

14. Vernant, P., Nilforoushan, F., Haztfeld, D., Abassi. M., Vigny, C., Masson, F., Nankali, H., Martinod, J., Ashtiany, A., Bayer, R., Tavakoli, F., and Chéry, J., (2004). "Contemporary Crustal Deformation and Plate Kinematics in Middle East Constrained by GPS Measurement in Iran and Northern Oman", *Geophys. J. Int.*, **157**, 381-398.

15. Jackson, J.A. (1992). "Partionning of Strike-Slip and Convergent Motion between Eurasia and Arabia in Eastern Turkey and Caucasus", *J. Geophys. Res.*, **97**, 12471-12479.

16. Talebian, M. and Jackson, J. (2004). "A Reappraisal of Earthquake Focal Mechanisms and Active Shortening in the Zagros Mountains of Iran", *Geophys. J. Int.*, **156**, 506-526.

17. Tchalenko, J.S. and Braud, J. (1974). "Seismicity and Structure of Zagros (Iran): the Main Recent Fault between 33° and 35°N", *Phil. Trans. Roy. Soc. Lond.*, **277**, 1-25.

18. Talebian, M. and Jackson, J. (2002). "Offset on the Main Recent Fault of the NW Iran and Implications for the Late Cenozoic Tectonics of the Arabia-Eurasia Collision Zone", *Geophys. J. Int.*, **150**, 422-439.

19. Falcon, N.L. (1969). "Problem of the Relationship between Surface Structures and Deep Displacement Illustrated by the Zagros Range", In: Time and Place Orogeny (Kent, P. Satterwaite, G., and Spencer, A., eds.), *Spec. Publ. Geol. Soc.*, London, **2**, 9-22.

20. Morris, P. (1977). "Basement Structure as Suggested by Aeromagnetic Surveys in SW Iran", *Second Geological Symposium of Iran*, Iranian Petroleum Institute, Tehran.

21. Talbot, C.J. and Alavi, M. (1996). "The Past of a Future Syntaxis Across the Zagros", *In: Alsop.*

G. I., (Blundell, D. J. and Davison, I, eds.), Geol. Soc. Spec. Publ., **100**, 89-110.

22. Sherkati, S. and Letouzey, J. (2004). "Variation of Structural Style and Basin Evolution in the Central Zagros (Izeh Zone and Dezful Embayement), Iran, *Geology*, **21**, 535-554.

23. Maggi, A., Jackson, J., Priestley, K., and Baker, C. (2000). "A Re-Assessment of Focal Depth Distributions in Southern Iran, the Tien Shan and Northern India: Do Earthquakes Really Occur in the Continental Mantle?", *Geophys. J. Int.*, **143**, 629-661.

24. Yamini Far, F. (2003). "Etude Seismotectonique et Caractérisation de la Structure Lithosphérique des Deux Zones de Transition: La Ligne d'Oman et la Ligne Qatar-Kazerun (Iran)", Ph.D. thesis, Université Joseph Fourier, Grenoble, 207 p.

25. Berberian, M. and Tchalenko, J. (1976). "Earthquakes of the Southern Zagros (Iran): Bushehr Region", *Geol. Surv. Iran Mem.*, **39**, 343-370.

26. Berberian, M. (1981). "Active Faulting and Tectonics of Iran. In: Zagros-Hindu Kush-Himalaya Geodynamic Evolution (H.K. Gupta and F.M. Delany, ed.)", *Am. Geophys. Union, Geodyn. Ser.*, **3**, 33-69.

27. Pattison, R. and Takin, M. (1971). "Geological Significance of the Dezful Embayment Boundaries", National Iranian Oil Company, Report, 1166.

28. Kent, P.E. (1979). "The Emergent Hormuz Salt Plugs of Southern Iran", *J. Petrol. Geol.*, **2**, 117-144.

29. Carey, E. (1979). "Recherche Des Directions Principales de Contraintes Associées au Jeu D'une Population de Failles", *Rev. Geol. Dyn. Geogr. Phys.*, **21**, 57-66.

30. Sepehr, S. (2000). "The Tectonic Significance of the Kazerun Fault Zone, Zagros Fold-Belt, Iran", Ph.D. Thesis, Imperial College, University of London, 215p.

31. Hever, H.J. (1977). "Behbahan-Gachsaran Geological Map 1:250000, Oil Serv", Comp Iran, No. 20511.

32. Alavi, M., Navai, I., Yousefi, M., Sedaghat, M.E., and Hamzepour, B. (1996). "Borujen Geological Map 1:250000", *Geol. Surv. Iran*.

33. Ehsanbakhsh Kermani, M.H. (1996). "Ardal Geological Map 1:100000", *Geol. Surv. Iran*, No. 6153.

34. Sedaghat, M.E. and Shaverdi, T. (1997). "Sisakht Geological Map 1:100000", *Geol. Surv. Iran*, No. 6251.

35. Sedaghat, M.E., Usefi, M., Kavari, E., and Navai, I., (1997). "Borujen Geological Map 1:100000", *Geol. Surv. Min. Expl. Iran*, No. 6253.

36. Sedaghat, M.E. and Gharib, F. (1999). "Dena Geological Map 1:100000", *Geol. Surv. Iran*, No. 6948.

37. Sedaghat, M.E., Gharib, F., and Shaverdi, T. (1999). "Semirom Geological Map 1:100000", *Geol. Surv. Iran*, No. 6352.

38. Jackson. J.A. and McKenzie, D.P. (1984). "Active Tectonics of the Alpine Himalayan Belt between Western Turkey and Pakistan", *Geophys. J. R. Astr. Soc.*, **77**, 185-264.

39. McQuarrie, N. (2004). "Crustal Scale Geometry of the Zagros Fold-Thrust Belt, Iran", *J. Struct. Geol.*, **26**, 519-535.

40. Almasiyan, M. (1992). "Tectonic and Seismo-Tectonic of Dena-Zagros Tear Zone in the Borujen Area", M.Sc.Thesis, Azad University, Tehran.

41. Ricou, L.E. (1976). "Evolution Structurale Des Zagrides, la Region Clef de Neyriz (Zagros Iranien), Mém. Soc. Geol. Fr., **55**, 1-140.

42. Hessami, K., Koyi, H.A., Talbot, C.J., Tabasi, H., and Shabanian, E. (2001). "Progressive Unconformities within an Evolving Foreland Fold-Thrust Belt, Zagros Mountains", *Geol. Soc. London*, **158**, 969-981.

43. Wells, A.J. (1969). "The Crush Zone of the Iranian Zagros Mountains, and Its Implications", *Geol. Mag.*, **106**, 385-394.

44. Westaway, R. (1994). "Present-Day Kinematics of the Middle-East and Eastern Mediterranean",

J. Geophys. Res., **99**, 12071-12090.

45. Axen, G.J., Lam, P.S., Grove, M., Stockli, D.F., and Hassanzadeh, J. (2001). "Exhumation of the West-Central Alborz Mountains, Iran, Caspian Subsidence, and Collision-Related Tectonics", *Geology*, **29**, 559-562.

46. Allen, M., Jackson, J., and Walker, R. (2004). "Late Cenozoic Re-Organization of the Arabia-Eurasia Collision and the Comparison of Short-Term and Long-Term Deformation Rates", *Tectonics*, **23**, TC2008, doi:10.1029/2003TC001530.

47. Regard, V., Bellier, O., Thomas, J.-C., Abbassi, M.R., Mercier, J.L., Shabanian, E., Feghhi, K., and Soleymani, S. (2004). "The Accommodation of Arabia-Eurasia Convergence in the Zagros-Makran Transfer Zone, SE Iran: A Transition between Collision and Subduction Through a Young Deforming System", *Tectonics*, **23**, doi:10.1029/2003TC001599.

48. Gidon, M., Berthier, F., Billiaud, J.P., Halbronn, B., and Maurizot, P. (1974). "Charriages et Mouvements Sédimentaires Tertiaires Dans la Région de Borudjerd (Zagros, Iran)", C.R. Acad. Sc. Paris, **278**, 421-424.

49. Hessami, K., Koyi, H.A., and Talbot, C.J. (2001). "The Significance of Strike-Slip Faulting in the Basement of the Zagros Fold and Thrust Belt", *J. Petrol. Geol.*, **24**, 5-28.

50. Blanc, E.J.-P., Allen, M.B., Inger, S., and Hassani, H. (2003). "Structural Styles in the Zagros Simple Folded Zone, Iran", *Geol. Soc. London*, **160**, 401-412.

51. NEIC, USGS National Earthquake Information Center Catalog (2002). Online Data Set: LIENHYPERTEXTE, http://wwwneic.cr.usgs.gov/neic/epic/epic.html.

52. Enkin, R.J. (1994). "A Computer Program Package for Analysis and Presentation of Paleomagnetic Data-PMSTAT", Vol. 1995, Pacific Geoscience Center, Geol. Survey Canada, Box 6000, Sidney, B.C., Canada, V8L 4B2.